

Escape of an Active Ring from an Attractive Surface: Behaving Like a Self-Propelled Brownian Particle

Bin Tang¹, Jin-cheng Gao¹, Kang Chen^{1*}, Tian Hui Zhang^{1*}, Wen-de Tian^{1*}

1. Center for Soft Condensed Matter Physics and Interdisciplinary Research, Soochow University, Suzhou 215006, China

Email: tianwende@suda.edu.cn, kangchen@suda.edu.cn, zhangtianhui@suda.edu.cn.

Abstract

Escape of active agents from metastable states are of great current interest in statistical and biological physics. In this study, we find that a flexible active Brownian ring escapes from a flat attractive surface though two distinct mechanisms: Kramers-like thermal activation at large rotational diffusion coefficients, but with an effective temperature, and the first-passage process at small rotational diffusion coefficients. The escape time depends explicitly on the shape of potential barrier at large activity and small rotational diffusion coefficient. Moreover, when the propulsion force was biased along its contour, escape becomes more difficult and is primarily caused by thermal noise. Our findings highlight that, despite its intricate configuration, the active ring can be considered an active Brownian particle when studying its escape from a smooth surface.

Introduction

The escape of a Brownian particle over a potential barrier is a thermally activated process, a classic problem known as Kramers' problem. [1] Kramers' theory [2] suggested that in the limit of vanishing particle flux across a potential barrier, the escape rate decreases exponentially with the increase of barrier height. Recently, active particles, which can convert environmental energy into directed motion, have attracted significant attention because they are inherently out of equilibrium. [3] Due to self-propulsion, active particles are expected to escape a potential barrier at a higher rate than passive particles. Activated escapes play a vital role in many physical phenomena, such as motility-induced phase separation and escape through narrow channels. [4] Although the coupling of orientational and positional degrees of freedom in active particles makes the theoretical treatment of the escape problem challenging, theorists have made significant efforts in both near-equilibrium and far-from-equilibrium regimes. [5–8]. For instance, Woillez et al. [9] found that the escape time of self-propelled Brownian particles is affected not only by the entire shape of the potential, but also by the height of the potential barrier. Caprini et al. [10,11] discovered that the velocity distribution of active particles around the potential barrier exhibits a bimodal shape in large persistence regimes.

Apart from point-like active particles, there exhibits chain or filament-like structures, usually termed active polymers [12], such as filamentous actin or microtubules of the cell cytoskeleton propelled by tread-milling and motor proteins. [13] Computer simulation [14,15] and theoretical studies [16–18] have shown that flexible linear active Brownian polymers swell upon the increasing of activity, and their overall diffusive dynamics are enhanced. Active Brownian rings have also received much attention due to their relevance in biological systems. [19] For example, the properties of ring-like DNA molecules are affected by ATP-dependent enzymatic activity, which induces mechanical fluctuations in the cytoplasm of eukaryotic cells. [20] Dynamically, the mean square displacement of an active Brownian ring exhibits ballistic, sub-diffusive, and diffusive regimes, indicating a distinct activity-enhanced diffusion. [19]

An interesting question arises: what does the escape of active Brownian ring behave? The motivation is threefold: First, from a physical perspective, tightly linked active particles are associated with persistent active stresses, unlike individual active particles. [17] These stresses affect the conformational and dynamical properties of active polymers, thereby altering their escape behaviors. Second, the escape behavior of biopolymers in confined environments is crucial for the survival and development of organisms. [21] Third, a typical escape phenomenon in polymer physics is the interfacial adsorption and desorption, which has numerous applications in industry and biomedicine. [22] As known, a complete escape of a polymer is unlikely to occur because of the small possibility for all segments to detach at the same time. To promote escaping, the method of "increasing temperature" is often adopted [23], where escape is driven by the increasing configurational entropy of the chain, counteracting the enthalpy from polymer-surface interactions. In contrast to thermal noise, the "active" force introduces activity to polymers. However, how this "activity" influences escape behavior remains an open question.

In this study, we investigate the escape of an active Brownian ring (ABR) from an attractive surface. Our results reveal that the escape time and activity follow an exponential decay at moderate activities within the framework of effective temperature, similar to Kramers' thermal activation mechanism. The escape time deviates from the exponential decay at higher activities due to the escape time being shorter than the timescale of the ballistic regime. Moreover, we investigated the effects of the rotational diffusion coefficient and the potential barrier. The critical barrier non-monotonically depends on the rotational diffusion coefficient, D_R (or, the persistence time), due to the existence of two escape mechanisms for small and large D_R s: thermal activity and the first-passage process. Additionally, we found that at large D_R s, the escape time weakly depends on the barrier shape, but at small D_R s, the shape plays a crucial role in escape dynamics, since it determines the maximal force that the ring must overcome. Furthermore, we observed that the driven mode also affects the escape. When the active force

was biased along its contour, the escape becomes difficult and is mainly aroused by background noise. Our findings suggest that the escape of ring-like structures can be understood as that of an active Brownian particle.

Model and methods

We perform Brownian dynamics (BD) simulations to investigate the behavior of a ring-like chain near an attractive homogeneous surface. The ring is formed by connecting N active Brownian monomers by bead-spring model often used in polymer physics. For an active Brownian ring (ABR), the intrinsic orientation \hat{q} of each monomer is random initially. A propulsive force $\mathbf{F}_a = F_a \hat{q}$ is applied along the \hat{q} , as shown in Fig. 1(a), where F_a is a constant magnitude.

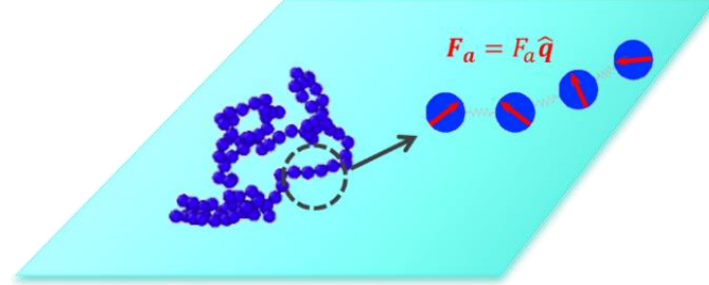


Fig. 1 Schematic illustration of an active Brownian ring (ABR) adsorbed on an attractive surface. Arrows indicate the directions of the active forces exerted on each monomer.

In our model, the total interaction U_{tot} is divided into three parts: the interaction between monomers U_{WCA} , the bond interaction between adjacent monomers U_b , and the attractive potential U_s .

$$U_{tot} = U_{WCA} + U_b + U_s \quad (1)$$

Here $U_{WCA} = \sum_{i < j}^N U(r_{ij})$ is represented by the pure repulsive WCA potential given below

$$U(r_{ij}) = \begin{cases} 4\epsilon \left[\left(\frac{\sigma}{r_{ij}} \right)^{12} - \left(\frac{\sigma}{r_{ij}} \right)^6 \right] + \epsilon & r_{ij} \leq 2^{1/6}\sigma \\ 0 & \text{otherwise} \end{cases} \quad (2)$$

where r_{ij} represents the distance between the i th and j th monomer. ϵ denotes the interaction strength and σ represents the diameter of monomer. The bond interaction U_b is expressed as $U_b = \frac{1}{2}k \sum_{i=1}^{N-1} (b_i - b_0)^2$ with spring coefficient $k = 2000.0k_B T/\sigma^2$. b_i denotes the i th bond length and $b_0 = \sigma = 1.0$ is the equilibrium-bond length.

To investigate the impact of shape of potential barrier $U_s = \sum_{i=1}^N U(z_i)$ on escape, three potential functions (U_1 , LJ-9-3; U_2 , harmonic; U_3 , Morse) were adopted with parameters adjusted to guarantee the same height of potential barriers at truncation distance $z_c = 3.0\sigma$. The three functions are listed below.

$$U_1(z_i) = \begin{cases} \epsilon_{s1} \left[\frac{2}{15} \left(\frac{\sigma}{z_i} \right)^9 - \left(\frac{\sigma}{z_i} \right)^3 \right] & z_i \leq z_c = 3.0\sigma \\ 0 & \text{otherwise} \end{cases}$$

$$U_2(z_i) = \begin{cases} -\epsilon_{s2} (z_i - z_c)^2 & 0.86\sigma \leq z_i \leq z_c = 3.0\sigma \\ \epsilon_{s1} \left[\frac{2}{15} \left(\frac{\sigma}{z_i} \right)^9 - \left(\frac{\sigma}{z_i} \right)^3 \right] & z_i \leq 0.86\sigma \\ 0 & \text{otherwise} \end{cases} \quad (3)$$

$$U_3(z_i) = \begin{cases} \epsilon_{s3} [e^{-2\alpha(z_i - z_0)} - 2e^{-\alpha(z_i - z_0)}] & 0.86\sigma \leq z_i \leq z_c = 3.0\sigma \\ \epsilon_{s1} \left[\frac{2}{15} \left(\frac{\sigma}{z_i} \right)^9 - \left(\frac{\sigma}{z_i} \right)^3 \right] & z_i \leq 0.86\sigma \\ 0 & \text{otherwise} \end{cases}$$

where ϵ_s is the attraction strength between monomer and surface, z_i is the distance between the i th monomer and surface. $z_0 = 0.86\sigma$ is the lowest point of the Morse potential.

The motion of ABR is described by the overdamped Langevin equations,

$$\gamma_T \frac{d\mathbf{r}(t)}{dt} = -\nabla U_{tot} + F_a \hat{q}(t) + \sqrt{6\gamma_T^2 D_T} \boldsymbol{\eta}_i^T \quad (4)$$

$$\frac{d\hat{q}(t)}{dt} = \sqrt{4D_R} \cdot \boldsymbol{\eta}_i^R \times \hat{q}(t) \quad (5)$$

Where γ_T denotes translational friction coefficient, $D_T (= \frac{k_B T}{\gamma_T})$ and D_R denote translational and rotational diffusion coefficient of monomers, respectively. $\boldsymbol{\eta}_i^T$ and $\boldsymbol{\eta}_i^R$, satisfying the fluctuation-dissipation theorem, denote the unit translational noise and rotational noise.

Generally, for spherical monomers, $D_T/D_R = \sigma^2/3$, but not obeyed in our simulation. D_T is kept constant at 1.0 and D_R is a parameter adjusted for studying its effects.

We used home-modified LAMMPS software to perform simulations of all systems. The equation of motions are solved by velocity-Verlet algorithm. An ABR is placed in a box of $100\sigma \times 100\sigma \times 50\sigma$. Periodic boundary conditions are used in x- and y- directions, the fixed boundary condition in z-direction. $N=100$, $T=1.0$, $\gamma_T = 1.0$, time step $dt = 10^{-4}\tau$ with $\tau = \sigma^2/D_T$. The dimensionless Péclet number (Pe) was defined as $Pe = F_a\sigma/k_B T$. Each simulation was performed with a long duration ($10^4\tau$) for data collection.

To analyze the structure and dynamics of the ring, the quantities such as the $Rg_{\parallel}^2(t)$ and $Rg_{\perp}^2(t)$ components of the mean square radius of gyration, the $MSD_{\parallel}(t)$ and $MSD_{\perp}(t)$ components of the mean square displacement (MSD) of its center of mass, the detached number of monomers $M(t)$, and the correlation function $G_c(t)$, are defined below (For details, please refer to [24]).

$$\begin{aligned}
x_{cm}(t) &= \frac{1}{N} \sum_{i=1}^N x_i(t), y_{cm}(t) = \frac{1}{N} \sum_{i=1}^N y_i(t), z_{cm}(t) = \frac{1}{N} \sum_{i=1}^N z_i(t) \\
Rg_{xy}^2(t) &= \frac{1}{N} \sum_{i=1}^N \{[x_i - x_{cm}]^2 + [y_i - y_{cm}]^2\}, Rg_z^2(t) = \frac{1}{N} \sum_{i=1}^N \{[z_i - z_{cm}]^2\} \\
MSD_{xy}(t) &= \langle (x_{cm}(t) - x_{cm}(0))^2 + (y_{cm}(t) - y_{cm}(0))^2 \rangle \\
MSD_z(t) &= \langle (z_{cm}(t) - z_{cm}(0))^2 \rangle \\
G_c(t) &= \langle \frac{N - M(t)}{N - M(0)} \rangle
\end{aligned} \tag{6}$$

Where $r_i(t) = [x_i(t), y_i(t), z_i(t)]$ and $r_{cm}(t) = [x_{cm}(t), y_{cm}(t), z_{cm}(t)]$, respectively, represent the coordinates of the i th monomer and the center-of-mass of the ring at time t . It should be noted that the re-adsorption is not considered when counting the monomers escaping from the surface. $\langle \dots \rangle$ represents the ensemble average of 1000 independent simulations. The escape time, τ_e , is obtained by fitting the correlation function $G_c(t) \sim \exp(-t/\tau_e)$. We systematically analyze the structure and dynamics of rings for the potential barrier $U_1(z_i)$ with $\varepsilon_{s1} = 5.0$ and present the results below, unless otherwise stated.

Results

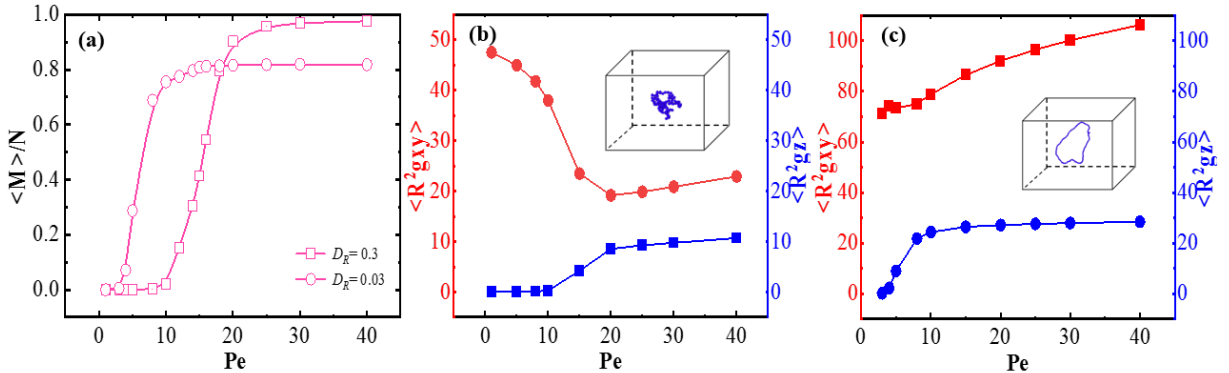


Fig.2. (a) The average numbers of escaped monomers $\langle M \rangle$ vary with Pe for $D_R = 3.0$ and 0.03 . (b) The xy- and z- components of radius of gyration as a function of Pe at $D_R = 3.0$. (c) The xy- and z- components of radius of gyration as a function of Pe at $D_R = 0.03$. The insets are snapshots for Pe=25.

Effect of activity

We first focus on the structure of ABR near the surface. The $\langle M \rangle$ s as functions of Pes for $D_R = 3.0$ and 0.03 are shown in Fig.2a. It can be found that for $D_R = 3.0$, at low activity, all monomers are adsorbed on the surface. At high activities, almost no monomers are adsorbed on the surface, indicating the escape of ABR (see Fig.S1 for $M(t)$). The result is qualitatively similar for $D_R = 0.03$, except that Pe becomes smaller for ABR escape. Thus, we conclude that an increase in activity can cause escape of ABRs from the attractive surface. This can also be manifested by the components of $\langle Rg^2 \rangle$ as functions of activities, as shown in Fig. 1b and Fig. 1c (Fig.S2) for $D_R = 3.0$ and 0.03 . For $D_R = 3.0$, $\langle Rg_{xy}^2 \rangle$ first decreases and then slightly increases with increasing Pe, in good agreement with the change in chain size in three dimensions with volume-excluded interactions[17]. Additionally, $\langle Rg_z^2 \rangle$ shows a monotonic increase with increasing Pe. In contrast, for $D_R = 0.03$, $\langle Rg_{xy}^2 \rangle$ monotonically increases with increasing Pe, accompanying the ABR escape. This implies that the escape of ring is accompanied by the fluctuation of chain conformation, which depends not only on the activity but also on the rotational diffusion coefficients.

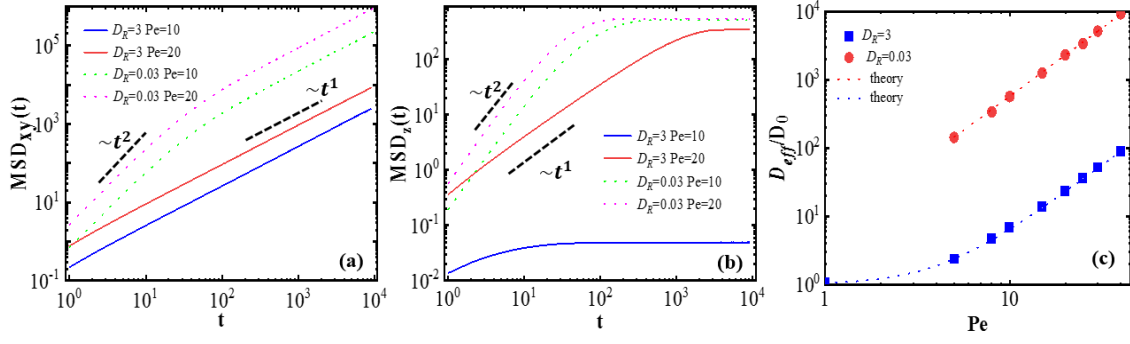


Fig.3. Time evolution of (a) $MSD_{xy}(t)$ and (b) $MSD_z(t)$. (c) The effective diffusion coefficients as a function of Pe . The dash lines are theoretical results ($D_{eff} = D_0(1 + aPe^2)$ with $D_0 = \frac{k_B T}{\gamma_T N}$ and $a = \frac{D_T^2}{\sigma^2 D_R}$).

Now we turn to the center-of-mass diffusion of ABR via the $MSD_{xy}(t)$ and $MSD_z(t)$, given in Fig.3a and Fig.3b. For $D_R = 3.0$, ballistic regime in the xy -direction is observed at very short times. When $Pe < 10$, sub-diffusion exists in the z direction due to ABR adsorbed on the surface. When $Pe \geq 20$, the ABR in the z -direction displays normal diffusion due to its escape from surface. For $D_R = 0.03$, the super-diffusion behavior at short time scales and normal diffusion at long time scales were observed in xy -directions for all Pe s, which is consistent with theoretical analysis. [25] It was suggested that the center-of-mass $MSD(t)$ in the bulk can be described by $MSD(t) = \frac{2dk_B T}{N\gamma_T}t + \frac{2v_0^2}{N(2D_R)^2}[(2D_R)t - 1 + e^{-(2D_R)t}]$. At short time scales, $MSD(t) = \frac{2dk_B T}{N\gamma_T}t + \frac{v_0^2}{N}t^2$. And, at long time scales, $MSD(t) = (\frac{2dk_B T}{N\gamma_T} + \frac{v_0^2}{ND_R})t$. Here $v_0 = P_e D_T / \sigma$ propulsion speed, d dimension. The crossover time between ballistic and diffusive motion is $\tau_c = 1/D_R$. By using Einstein's relation $MSD_{xy}(t) = 4D_{eff}t$, we get the effective diffusion coefficient of the ring (Fig.3c). The effective diffusion coefficient yields the function $D_{eff} = D_0(1 + aPe^2)$ with $a = \frac{D_T^2}{\sigma^2 D_R}$ and $D_0 = \frac{k_B T}{\gamma_T N}$, the diffusion coefficient of ABR at $Pe=0$. For $D_R = 3.0 = 3D_T$, a is close to the value, 1/18, of theoretical predication where the steric interaction is omitted. [25] It can be seen from Fig.3c that D_{eff} s from simulations agree well with theoretical values. According to the position fluctuations, one could define effective temperatures, T_{eff} , replacing the thermal temperature for the description of ABR' properties. The effective temperature of ring' center-of-mass is $T_{eff} = T(1 + aPe^2)$, where T is the thermal noise.

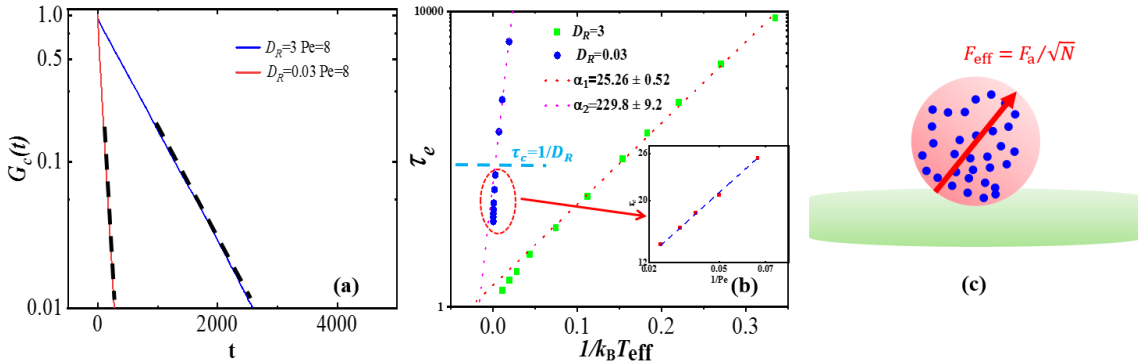


Fig.4. (a) The delay of $G_c(t)$ over time. The dash line is for eye-guiding fitting of $G_c(t) \sim \exp(-t/\tau_e)$. (b) Semi-log plot of τ_e as a function of $1/T_{eff}$. The blue and green dash lines represent the fitting curve using $\tau_e \sim \exp(\alpha/k_B T_{eff})$. The inset is τ_e as a function of $1/Pe$ for $D_R=0.03$ with large activities. The crossover time $\tau_c = 1/D_R$ between ballistic and diffusive motion for $D_R=0.03$ is also illustrated. (c) A sketch of active Brownian particle for the escape of an active Brownian ring from surface. The effective propulsion force is equal to F_a/\sqrt{N} .

Semi-log plot of $G_c(t)$ for various Pe s is shown in Fig.4a. It can be observed that $G_c(t)$ features a short transient period, where escape occurs rapidly, followed by an exponential decay described by $G_c(t) \sim \exp(-t/\tau_e)$ at long time scales. The linear region was fitted to obtain τ_e s. To understand the escape mechanism induced by the active force, the dependence of τ_e on T_{eff} is plotted semi-logarithmically in Fig.4b. For large $D_R (= 3.0)$, the escape time fits well with an exponential function, $\tau_e \sim \exp(\alpha/k_B T_{eff})$, with fitting parameter $\alpha \approx 25$. Here α is relevant to the average adsorption energy of ring. This indicates that the escape mechanism is similar to that of Brownian particles by thermal activation. For small $D_R (= 0.03)$, there are evidently two regimes: when $Pe < 10$, the escape time fits well with $\tau_e \sim \exp(\alpha/k_B T_{eff})$ with $\alpha \approx 230$. However, when $Pe > 10$, τ_e decreases sharply with increasing Pe compared to the exponential decay,

and it can be nearly fitted by $\tau_e \sim P_e^{-1}$. These findings can be understood as follows: without steric interactions among monomers, which do not greatly affect the escape of the entire ring, the ring can be considered an active sphere composed of N monomers (Fig.4c). [25] The sphere has an effective thermal diffusion coefficient of D_T/N and an effective propulsion velocity of v_0/\sqrt{N} . The persistence time $\tau_R = 1/(2D_R)$ is the same as that of each monomer. Thus, the escape process of the active Brownian ring (ABR) is intuitively similar to that of an active Brownian sphere. When $\tau_e > \tau_c$, the escape is a thermally activated process with an effective temperature T_{eff} . When $\tau_e < \tau_c$, the sphere behaves in a ballistic manner, and the escape time is the ratio of the barrier's width to the effective propulsion velocity. Meanwhile, in the regime, the propulsion force is larger than that by potential barrier. This physical picture is in line with what we find here.

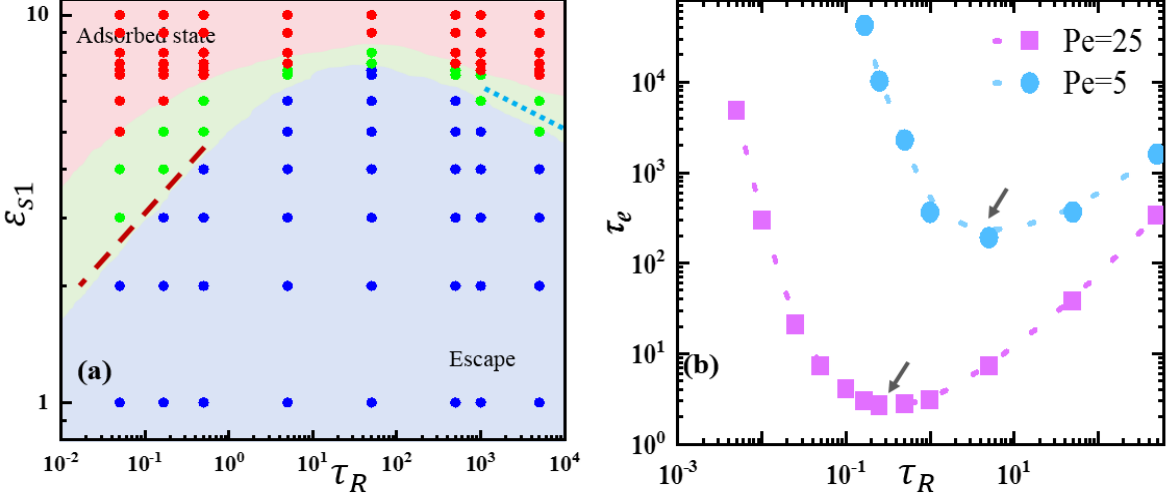


Fig. 5 (a) $\varepsilon_{s1} - \tau_R$ phase diagram for $\text{Pe}=5$. $\tau_R = 1/2D_R$ is persistence time of monomer. Red points denote adsorbed states, blue escape, and the green intermediate regime. The dash lines are for eye-guiding phase boundary (b) τ_e as a function of τ_R for $\text{Pe} = 25$ and 5. The arrows point to the optimal persistence time.

$\tau_R - \varepsilon_{s1}$ Phase diagram

τ_e s are different at various D_R s, even with the same potential barrier and activity, which counteract with each other in terms of escaping. To further understand the influence of D_R , $\varepsilon_{s1} - \tau_R$ phase diagram is shown in Fig.5a for $\text{Pe}=5$. $\tau_R = 1/2D_R$ is the persistence time of each monomer. Clearly, two states can be distinguished by τ_e . For an escape state, τ_e is less than our simulation time ($10^4\tau$). For an adsorbed state, τ_e is too larger to be fitted. Additionally, an intermediate regime is defined when τ_e can be fitted but is larger than our simulation time. At a certain activity, the high barrier leads to adsorbed states, while for low barriers, escape occurs regardless of τ_R due to the existence of background noise.

At the phase boundary, the critical barrier first increases and then decreases with the increase of τ_R . This originates from the different escape mechanisms at small and large τ_R s, which can be manifested by τ_e as a function of τ_R . As shown in Fig.5b, τ_e decreases first and then increases with τ_R . For small τ_R s, the monomers rotate quickly. The whole ring behaves like a passive one with temperature T_{eff} , thus $\ln \tau_e \sim \alpha/\tau_R$. That's why τ_e decreases as τ_R grows at first. For large τ_R s, the escape occurs almost deterministically when the magnitude of the active force exceeds the maximal force by the potential barrier, because the orientation of the active force has little chance to reverse its direction while crossing the barrier.[26] Hence, the escape time is almost equal to the waiting time for the occurrence of an active force exceeding the maximal force. The barrier crossing becomes a first-passage process, the mean time of which $\sim \tau_R$ (Equation 5). As a result, the larger of τ_R implies the larger escape time. [26] Additionally, the remarkable non-monotonic behavior demonstrates that, for a given Pe, there exists an optimal τ_R . The optimal τ_R can be roughly estimated by the ratio of barrier width and propulsive velocity, meaning that it is inversely proportional to activity. Indeed, the optimal τ_R at $\text{Pe}=10$ is smaller than that at $\text{Pe}=5$ (Fig.5b). The finding qualitatively agrees with that of Caprini et al. [11], who studied the escape of an active Brownian particle from a double-well potential.

The non-monotonicity of critical barriers at the same activity caused by two escape mechanisms can be explained below. In the regime of small τ_R s, the activated noise dominates. Critical barriers are estimated by $\sim k_B T_{\text{eff}}$. Since $T_{\text{eff}} \propto \frac{v_0^2}{ND_R} \propto \tau_R$, we obtain the critical barriers increase with τ_R . In the regime of large τ_R s, first-passage process dominates. Larger τ_R means a longer waiting time to reach the maximum force. Therefore, at the limited waiting time (our simulation time is $10^4\tau$) and fixed Pe, critical barrier decreases with the increase of τ_R .

Effect of barrier shape

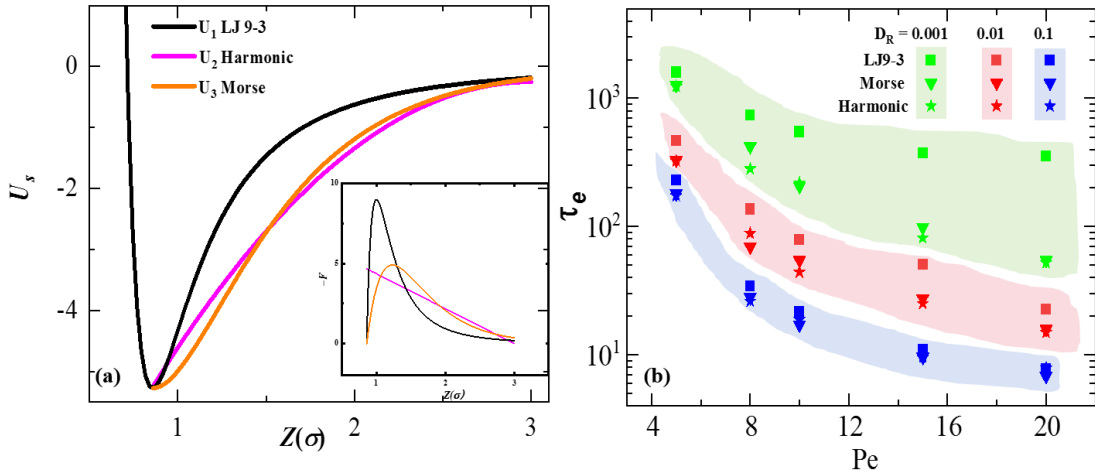


Fig. 6. (a) The shapes of the three barriers: Harmonic potential, LJ9-3 potential, and Morse potential with $\varepsilon_{s1} = 5.0$, $\varepsilon_{s2} = 1.09$, and $\varepsilon_{s2} = 5.27$. The inset is the corresponding force. (b) The escape times as functions of Pe for the three barriers with various D_R s.

Now we are interested in the effect of the shapes of the potential barriers on ABR's escape. To realize the different potential shapes, the attractive region of LJ-9-3 potential (U_1) was replaced by that of harmonic (U_2) and Morse potential (U_3). The shapes of potentials and forces are plotted in Fig.6a. To study the effect of barrier's shape, we keep the heights of three barriers are nearly same, $\Delta U \approx 5.0k_B T$, in the range of z from 0.86σ to 3.0σ . The escape time as a function of activity for three D_R s ($=0.1, 0.01, 0.001$) is presented in Fig.6b. For large D_R ($=0.1$, blue background), the escape times for the three barriers are very close for all Pe values, implying that the escape weakly depends on the barrier shapes because the thermally activated mechanism is dominant here. The behavior is similar for small Pe ($=4.0$). At small D_R ($=0.001$, blue background) and large Pes, the deviation in escape time becomes significantly large, especially for the LJ-9-3 potential. This indicates that the barrier shape indeed impacts the escape time of ABR at the large persistence length of monomers, similar to the finding of Woillez et al. [9], who studied the noise-driven escape of active Brownian particles. The reason might be that the maximal trapping force exerted by different barrier shapes on the monomer is different. The maximal trapping force of LJ-93 potential is larger than that of the other two potentials.

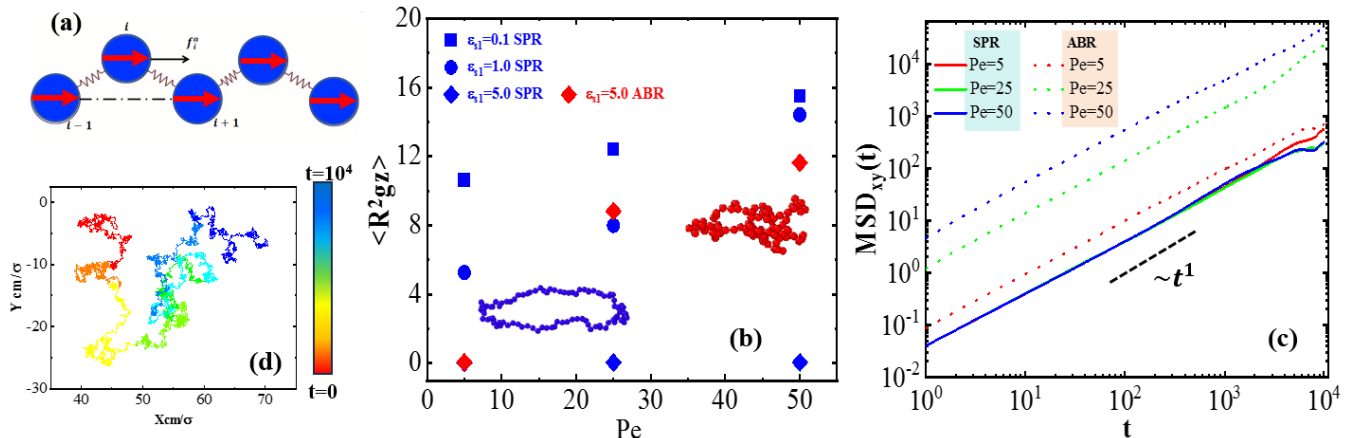


Fig. 7. (a) Sketch of self-propelling ring (SPR). (b) $\langle Rg_z^2 \rangle$ as a function of Pe for various ε_{s1} s. The $\langle Rg_z^2 \rangle$ s of ABR for $\varepsilon_{s1} = 5.0$ are also given for comparison. The insets are typical snapshots for SPR (blue beads) and ABR (red beads) at $\varepsilon_{s1} = 5.0$, Pe = 50. (c) MSD of SPRs and ABRs for various activities at $\varepsilon_{s1} = 5.0$. (d) The time evolution of trajectory for the center-of-mass of SPR, and those of ABR are also given for comparison.

Effect of propulsive mode

For active Brownian ring, the orientations of monomers do not associate with chain conformation, so the whole chain behaves like an active Brownian sphere. The interesting question is how the coupling of propelling directions and chain configuration affects escape behavior. Now we restrict their orientations along with the contour of the ring, i.e., biasing the orientations to preferentially align with the instantaneous tangent vector of ring's contour through a potential $\frac{K}{k_B T}(\hat{\mathbf{n}}_i - \hat{\mathbf{b}}_i)^2$, were $\hat{\mathbf{b}}_i = \frac{\mathbf{r}_{i+1,i-1}}{|\mathbf{r}_{i+1,i-1}|}$ is the i th vector, K is the biasing strength. In the following, we only discuss the case of strong restriction ($K \rightarrow \infty$), that is often called the self-propelling ring (SPR), a sketch of which is

given in Fig.7a.

The $\langle Rg_z^2 \rangle$ s as a function of Pe are shown in Fig.7b. The value of $\langle Rg_z^2 \rangle$ close to zero means the SPR adsorbs on the surface, otherwise, it escapes from the surface. For $\varepsilon_{s1} = 5.0$, the $\langle Rg_z^2 \rangle$ of ABR are also given for comparison. It can be found that, the escape of SPR occurs at the attractive strengths near or below $\varepsilon_{s1} \leq 1.0$ (see Fig.S3 for the distribution of monomers along the z direction). ABR is relatively easy to escape at the same activities and attractive barriers. It implies that the propulsive mode impacts the escape dynamics of ring. To understand why the SPR is hard to escape from the flat surface. We calculate the $MSD_{xy}(t)$ s of its center of mass at various activities. As seen in Fig.7c, the increase in the magnitude of active force seems not to increase the effective diffusion coefficients. The behavior significantly differs with that of ABR, the effective diffusion coefficient of which increase with active force. It can be also witnessed by the time evolution of the center-of-mass position of SPR (Fig.7d), which shows an diffusive motion on the surface. This implies that the escape of SPR is mainly caused by the environmental noise with the strength, T . Theoretically (please see SI for details), the SPR can be represented continuously for long chain. Then the resultant force on the center of mass is proportional to $F_a \mathbf{R}_E$, which is zero due to the end-to-end vector $\mathbf{R}_E = 0$ for ring-like chain. Hence, the $MSD(t) = \frac{2dD_T}{N}$ irrelevant to the active force. This implies that the escape of SPR is like that of passive particles, i.e., the active Brownian particles with Pe=0.

Summary and discussion

We explored the escape of a flexible active Brownian ring on a flat attractive surface by computer simulations. At low activity, an adsorbed state with ABR diffusing on the surface exists. High activity gives rise to the escape of active ring. The diffusion behavior of ABR parallel to the surface is in good agreement with that predicated by theory. Hence, an effective temperature, $T_{\text{eff}} = T(1 + aPe^2)$, can be defined due to the existence of non-thermal active noise. The escape kinetics was measured by the escape time τ_e through linear fitting $G_c(t) \sim \exp(-t/\tau_e)$. Our results reveals that the escape time τ_e and Pe follows an exponential decay, $\tau_e \sim \exp(\alpha/k_B T_{\text{eff}})$, at moderate activity, similar to the mechanism of thermal activation. Interestingly, we also found the deviation of escape time from the exponential decay at larger Pes due to the escape time smaller than time scale of ballistic regime, where the escape behaves like a constant-speed running away. Moreover, we investigated the effect of rotational diffusion coefficient and potential barrier. The phase diagram is given and we observed a non-monotonic dependence of escape time on the D_R and perceived there exists an optimal D_R for the chain escape.

We also focus on the shape of potential barriers and find that at large D_R s, the escape time weakly depends on the shape, but at small D_R s, the shape plays a crucial role in escape dynamics, as it determines the maximal force the ring must overcome. Additionally, we find that the mode of propulsion also affects escape behavior. For self-propelling rings, escape is difficult due to the active force along the contour, and escape is mainly induced by background noise.

It should also be noted that this study is a first step toward understanding activity-induced escape of chain-like active structures. Another interesting question is exploring the effect of the inertia of each monomer using underdamped Langevin dynamics. Our findings suggest that ring-like structures can be considered as active Brownian particles when studying their escape from a smooth surface. However, escaping from a cavity or passing through a pore with geometry confinement might be very different due to configuration entropy, making it a topic worth further study.

SUPPLEMENTARY MATERIAL

See the supplementary material for additional details....

ACKNOWLEDGMENTS

Project supported by the National Natural Science Foundation of China of Grant Nos. 21674078 (Tian), 21774091 (Chen), and 21574096(Chen).

DATA AVAILABILITY

The data that support the findings of this study are available from the corresponding author upon reasonable request

REFERENCES

[1] D. Wang, H. Wu, L. Liu, J. Chen, and D. K. Schwartz, *Diffusive Escape of a Nanoparticle from a Porous Cavity*, Phys. Rev. Lett. **123**, 118002 (2019).

[2] E. Pollak and S. Miret-Artés, *Recent Developments in Kramers' Theory of Reaction Rates*, *ChemPhysChem* **24**, e202300272 (2023).

[3] O. Chepizhko and F. Peruani, *Active Particles in Heterogeneous Media Display New Physics*, *The European Physical Journal Special Topics* **224**, 1287 (2015).

[4] Y. Fily and M. C. Marchetti, *Athermal Phase Separation of Self-Propelled Particles with No Alignment*, *Phys. Rev. Lett.* **108**, 235702 (2012).

[5] I. S. Aranson and A. Pikovsky, *Confinement and Collective Escape of Active Particles*, *Phys. Rev. Lett.* **128**, 108001 (2022).

[6] D. Wexler, N. Gov, K. Ø. Rasmussen, and G. Bel, *Dynamics and Escape of Active Particles in a Harmonic Trap*, *Phys. Rev. Research* **2**, 013003 (2020).

[7] A. Das, B. Kuznets-Speck, and D. T. Limmer, *Direct Evaluation of Rare Events in Active Matter from Variational Path Sampling*, *Phys. Rev. Lett.* **128**, 028005 (2022).

[8] A. Militaru, M. Innerbichler, M. Frimmer, F. Tebbenjohanns, L. Novotny, and C. Dellago, *Escape Dynamics of Active Particles in Multistable Potentials*, *Nat Commun* **12**, 2446 (2021).

[9] E. Woillez, Y. Zhao, Y. Kafri, V. Lecomte, and J. Tailleur, *Activated Escape of a Self-Propelled Particle from a Metastable State*, *Phys. Rev. Lett.* **122**, 258001 (2019).

[10] L. Caprini, U. Marini Bettolo Marconi, A. Puglisi, and A. Vulpiani, *Active Escape Dynamics: The Effect of Persistence on Barrier Crossing*, *The Journal of Chemical Physics* **150**, 024902 (2019).

[11] L. Caprini, F. Cecconi, and U. Marini Bettolo Marconi, *Correlated Escape of Active Particles across a Potential Barrier*, *The Journal of Chemical Physics* **155**, 234902 (2021).

[12] R. G. Winkler, J. Elgeti, and G. Gompper, *Active Polymers — Emergent Conformational and Dynamical Properties: A Brief Review*, *J. Phys. Soc. Jpn.* **86**, 101014 (2017).

[13] J. Chan, G. Calder, S. Fox, and C. Lloyd, *Cortical Microtubule Arrays Undergo Rotary Movements in *Arabidopsis* Hypocotyl Epidermal Cells*, *Nat Cell Biol* **9**, 171 (2007).

[14] S. Paul, S. Majumder, and W. Janke, *Activity Mediated Globule to Coil Transition of a Flexible Polymer in a Poor Solvent*, *Soft Matter* **18**, 6392 (2022).

[15] V. Bianco, E. Locatelli, and P. Malgaretti, *Globule-like Conformation and Enhanced Diffusion of Active Polymers*, *Phys. Rev. Lett.* **121**, 217802 (2018).

[16] S. Chaki and R. Chakrabarti, *Enhanced Diffusion, Swelling, and Slow Reconfiguration of a Single Chain in Non-Gaussian Active Bath*, *The Journal of Chemical Physics* **150**, 094902 (2019).

[17] A. Kaiser, S. Babel, B. ten Hagen, C. von Ferber, and H. Löwen, *How Does a Flexible Chain of Active Particles Swell?*, *The Journal of Chemical Physics* **142**, 124905 (2015).

[18] A. Kaiser and H. Löwen, *Unusual Swelling of a Polymer in a Bacterial Bath*, *J. Chem. Phys.* **141**, 044903 (2014).

[19] E. Locatelli, V. Bianco, and P. Malgaretti, *Activity-Induced Collapse and Arrest of Active Polymer Rings*, *Phys. Rev. Lett.* **126**, 097801 (2021).

[20] R. Takaki, A. Dey, G. Shi, and D. Thirumalai, *Theory and Simulations of Condensin Mediated Loop Extrusion in DNA*, *Nat Commun* **12**, 5865 (2021).

[21] P. Jun Park and W. Sung, *Dynamics of a Polymer Surmounting a Potential Barrier: The Kramers Problem for Polymers*, *The Journal of Chemical Physics* **111**, 5259 (1999).

[22] N. Källrot and P. Linse, *Dynamic Study of Single-Chain Adsorption and Desorption*, *Macromolecules* **40**, 4669 (2007).

[23] Y. Wang, R. Rajagopalan, and W. L. Mattice, *Kinetics of Detachment of Homopolymers from a Solid Surface*, *Phys. Rev. Lett.* **74**, 2503 (1995).

[24] G. Feng and W. Tian, *Desorption of a Flexible Polymer with Activity from a Homogeneous Attractive Surface*, *Macromolecules* **56**, 2542 (2023).

[25] S. M. Mousavi, G. Gompper, and R. G. Winkler, *Active Brownian Ring Polymers*, *J. Chem. Phys.* **150**, 064913 (2019).

[26] E. Woillez, Y. Kafri, and V. Lecomte, *Nonlocal Stationary Probability Distributions and Escape Rates for an Active Ornstein-Uhlenbeck Particle*, *J. Stat. Mech.* **2020**, 063204 (2020).

Supporting Information (SI)

A: Supporting Figures

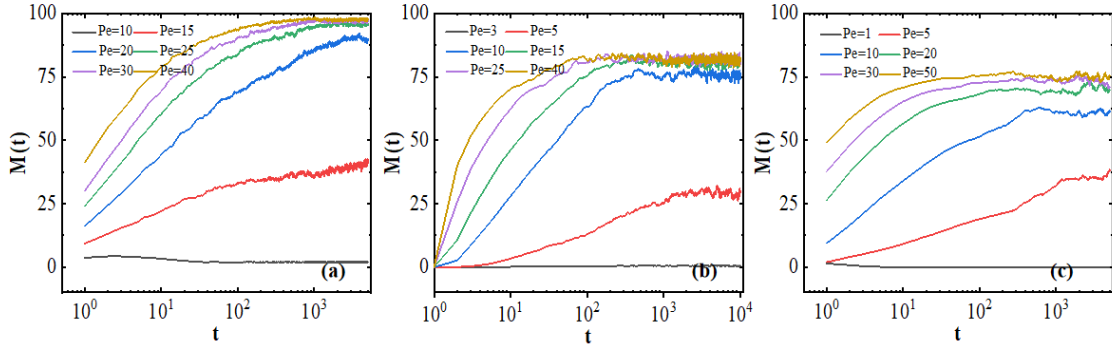


Fig.S1. Time evolution of escaped agents $M(t)$ vary with Pe for $N=100$ and $\varepsilon_{s1} = 5.0$, the truncated 9-3 Leonard-Jones potential is used. (a),(b) and (c) represent the results of $D_R = 3, 0.03$ and 0.001 , respectively. When the activity is small ($Pe \leq 10$), the number of escaped monomers is almost 0, and with the increase of activity, the number of escaped monomers gradually increased and approached 100, indicating that activity caused the escape of monomers.

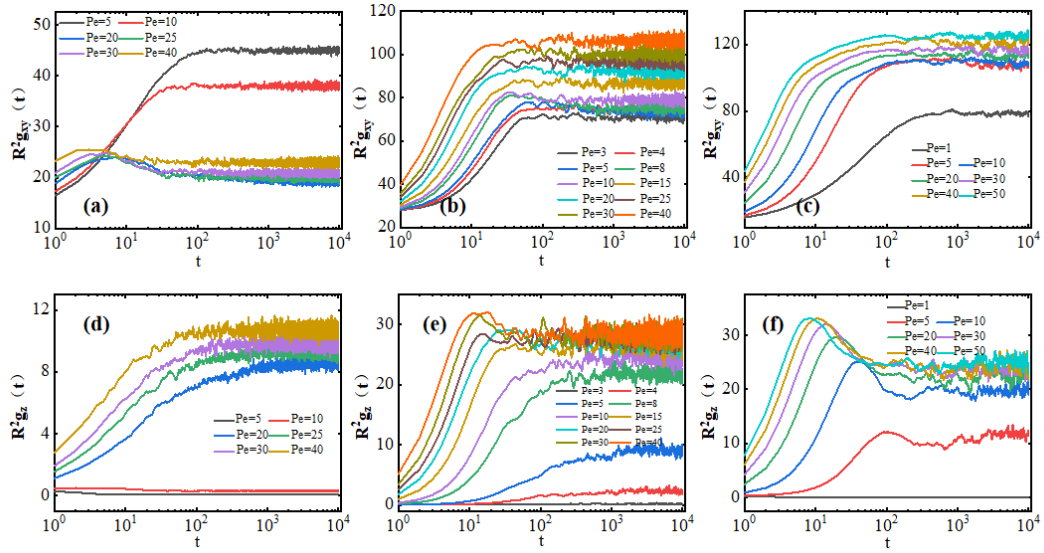


Fig.S2: Time evolution of $Rg_{xy}(t)$ and $Rg_z(t)$ vary with Pe for $N=100$ and $\varepsilon_{s1} = 5.0$, the truncated 9-3 Leonard-Jones potential is used. (a)(d),(b)(e) and (c)(f) represent the results of $D_R = 3, 0.03$ and 0.001 , respectively. When $D_R = 3$, Rg_{xy}^2 showed a non-monotonic trend of first increasing and then decreasing under low activity, and gradually increased and tended to be stable with the increase of activity. For both $D_R = 0.03$ and 0.001 , Rg_{xy}^2 increased with the increase of activity. For the three kinds of D_R , Rg_z^2 in the z direction is close to 0 under low activity, and gradually increases with the increase of activity.

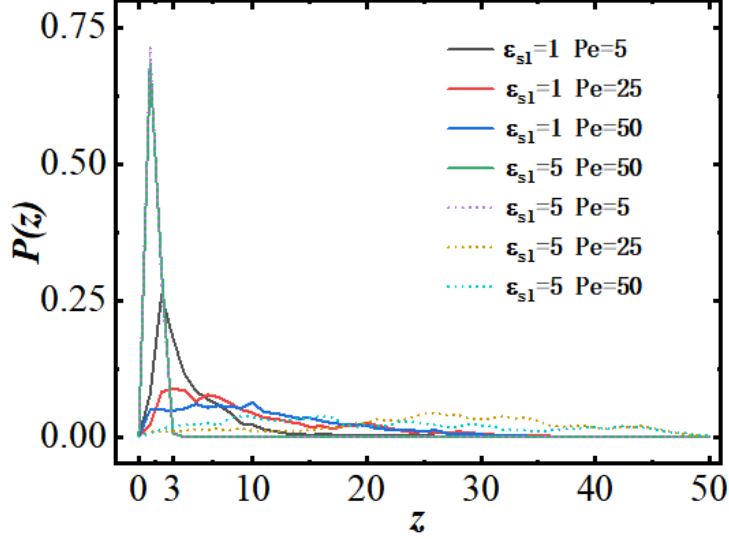


Fig.S3 :Probability distribution $P(z)$ of particles along the z direction. The solid line indicates the SPR, and the dashed line indicates the ABR. The probability distribution $P(z)$ of the monomer along the z direction shows that, when $\epsilon_{s1} = 5$, almost all monomers on self-propelling ring (solid line) cannot escape. With the decrease of attraction strength and the increase of activity, the peak value gradually moves to the right, and the chain gradually escapes from the interface. When $\epsilon_{s1} = 5$, for the active Brownian ring (dashed line), the peak of $P(z)$ gradually moves to the right with the increase of activity, showing obvious interface escape.

B. Theory for the dynamics of the SPR

To derive the dynamics of the center of mass of the SPR, we assume the equation is overdamped and ignore the attractive interaction of the surface. Then the equation for the i th agent can be written as

$$\dot{\mathbf{r}}_i = \frac{D_T}{k_B T} (-\nabla_i U + \mathbf{F}_i^a) + \boldsymbol{\eta}_i \quad (S2)$$

Where D_T is the translational diffusion coefficient, k_B is the Boltzmann constant, T is the temperature. $\boldsymbol{\eta}$ obeys the fluctuation-dissipation theorems with $\langle \boldsymbol{\eta}_i(t) \rangle = 0$ and $\langle \boldsymbol{\eta}_i(t) \cdot \boldsymbol{\eta}_j(t') \rangle = 2dD_T\delta(t-t')$. $d = 3$ is the dimension of system.

The equation of motion of center of mass is the summary of Equation (S2)

$$\dot{\mathbf{r}}_{com} = \frac{1}{N} \sum_{i=1}^N \dot{\mathbf{r}}_i = \frac{D_T}{Nk_B T} \sum_{i=1}^N (-\nabla_i U + \mathbf{F}_i^a) + \frac{1}{N} \sum_{i=1}^N \boldsymbol{\eta}_i = \frac{D_T}{Nk_B T} \mathbf{F}_T^a + \frac{1}{N} \boldsymbol{\eta}_T \quad (S3)$$

with the total active force $\mathbf{F}_T^a = \sum_{i=1}^N (\mathbf{F}_i^a) = F \sum_{i=2}^{N-1} \left(\frac{\mathbf{r}_{i+1} - \mathbf{r}_{i-1}}{|\mathbf{r}_{i+1} - \mathbf{r}_{i-1}|} \right)$ and the total thermal noise $\boldsymbol{\eta}_T = \sum_{i=1}^N \boldsymbol{\eta}_i$. The total random noise accounting for

the thermal fluctuation of the center of mass obeys $\langle \boldsymbol{\eta}_T(t) \rangle = 0$, $\langle \boldsymbol{\eta}_T(t) \cdot \boldsymbol{\eta}_T(t') \rangle = 2dND_T\delta(t-t')$. Because we do not consider the effect of surface, the resultant force from $\nabla_i U$ is equal to zero. For the convenience of theoretical analysis, we assume the SPR can be represented continuously, then the total active force \mathbf{F}_T^a is proportional the integral over the SPF backbone of the unit tangent vector, $\hat{\mathbf{l}}$,

$$\mathbf{F}_T^a = \frac{F}{b_0} \int_0^N \hat{\mathbf{l}} dl = \frac{F}{b_0} \mathbf{R}_E \quad (S4)$$

Where \mathbf{R}_E is the end-to-end vector of SPF. It should be noted that the above continuum representation of SPF is only valid for the long SPF, i.e., large N . It will be irrational for short polymers. For the ring-like structure, the $\mathbf{R}_E = 0$. Then we could get

$$\begin{aligned}
\langle \mathbf{r}_{cm}^2(t) \rangle &= \left(\frac{D_T F}{N k_B T b_0} \right)^2 \left\langle \iint \mathbf{R}_E(t') \cdot \mathbf{R}_E(t'') dt' dt'' \right\rangle + \left(\frac{1}{N} \right)^2 \left\langle \iint \boldsymbol{\eta}_r(t') \cdot \boldsymbol{\eta}_r(t'') dt' dt'' \right\rangle \\
&= \frac{2dD_T}{N} t
\end{aligned} \tag{S5}$$